Braz J Phys (2014) 44:719–725
DOI 10.1007/s13538-014-0270-2

CONDENSED MATTER

Characterization of Co-evaporated Cu-Ag-In-Se Thin Films

H. H. Güllü · E. Coşkun · M. Parlak

Received: 22 June 2014 / Published online: 8 October 2014

Abstract In this study, annealing effect on the structural, electrical, and optical characteristics of the quaternary Cu-Ag-In-Se (CAIS) thin films was investigated. These samples were deposited by co-evaporation of the Cu, Ag, In_2Se_3, and Se sources at the substrate temperature of 300 °C. The structural properties of the thin films were analyzed by means of X-ray diffraction, and the results indicated that all of the films were in the polycrystalline structure with the preferred orientation along (112) direction. From the optical measurements, the band gap values were found to vary between 1.38 and 1.45 eV with annealing processes. The temperature-dependent electrical conductivity of the samples was measured in the temperature range of 90–400 K. The films gained degenerate behavior with increasing annealing temperature. The carrier conduction mechanism was determined at high- and low-temperature regions by comparing thermionic emission and hopping parameters. Photoconductivity of the as-grown film showed that there was an increase in conductivity with increasing illumination intensity. From this measurement, the variation of photocurrent as a function of illumination intensity was determined.

Keywords Thin film · Thermal evaporation · Thermionic emission · Variable range hopping · Photoconductivity

H. H. Güllü (✉) · E. Coşkun · M. Parlak
Department of Physics, Middle East Technical University (METU), Ankara 06800, Turkey
e-mail: hgullu@metu.edu.tr

E. Coşkun
Department of Physics, Çanakkale Onsekiz Mart University, Çanakkale 17100, Turkey

H. H. Güllü · E. Coşkun · M. Parlak
Center for Solar Energy Research and Applications (GÜNAM), METU, Ankara 06800, Turkey

1 Introduction

The family of the chalcopyrite semiconductors in the group of $I–II–VI_2$ appears to be good candidate materials for solar cell applications due to having desired properties to be an absorber material. These ternary materials are the electron-chemical analogs of the II–VI binary structures and crystallize in the I42m space group [1]. Indeed, in recent years, the quaternary structures have been preferentially studied by different research groups due to the advantage of tailoring suitable values of lattice parameters and energy band gap with the proper choice of composition to reduce the disability of the constituent elements [2]. The Cu-based thin film structures can keep their characteristics stable against the changes in thermal, environmental, and electrical effects [3]; they have good light absorption characteristics with high absorption coefficients ($>10^4$ cm^{-1}) [4] and a good match with CdS [5, 6]. The maximum solar cell efficiency was obtained from the $Cu(In,Ga)Se_2$ quaternary alloy system. It was achieved by group III isoelectronic substitution of In by Ga. However, Cu atoms in the structure can cause shorting effect due to having high diffusion coefficient [7], and the research on group I substitution has been proceeded to eliminate this problem and, according to the studies, silver (Ag) is taking the great interest as a substitute for Cu [8].

In these quaternary structures, Cu-Ag-In-Se (CAIS) system is located between the ternary semiconducting chalcopyrite compounds $CuInSe_2$ (CIS) and $AgInSe_2$ (AIS). These are the two most popular materials applied in photovoltaic cells because of their high optical absorption coefficient, which is an important factor for the manufacture of devices, and their direct energy gap values are 1.05 eV (CIS) [9] and 1.24 eV (AIS) [10]. As it is known, very little work has been reported on the growth and characterization of CAIS thin film structures. Most of the works are related to structural [2, 9, 11], electrical [2, 12], and optical properties [1, 2, 8, 10, 12–15]

and also device behaviors [16, 17] of CAIS thin film deposited by different methods.

In this work, CAIS thin films were deposited by the thermal evaporation and systematic post-thermal annealing process was carried out to investigate its effect on the film characteristics.

2 Experimental Details

CAIS thin films were deposited by co-evaporation technique of the Cu, Ag, In_2Se_3, and Se evaporation sources by using Vaksis Midas-PVD system. During the deposition process, the substrate temperature was kept at about 300 °C. The evaporation sources were evaporated subsequently by applying layer by layer deposition technique, with deposition rates about 0.3 Å/s (Cu), 0.3 Å/s (Ag), 0.5 Å/s (In_2Se_3), and 1.0 Å/s (Se). These evaporation rates were controlled by Inficon XTM/2 deposition monitor, connected to the quartz crystal inside the vacuum chamber.

The thin films were characterized firstly in as-grown form, and then under the nitrogen atmosphere. The post-annealing was applied to some of the samples to deduce the effects of annealing on the film properties of the deposited samples. During the annealing process the temperature of the samples was kept at 350 and 400 °C for 60-min time interval.

The structural properties of the films were investigated by Rigaku Miniflex X-ray Diffraction (XRD) system, equipped with Cu-K_α X-ray source (λ=1.54 Å), and XRD scans were taken in the range of 10–90° with a scanning speed of 2° min^{-1}. The analysis of the surface morphology and elemental composition of the CAIS films were carried out in a JSM-6400 scanning electron microscope (SEM) equipped with EDAX. Transmission spectra in the wavelength range of 300–1100 nm were measured using Shimadzu UV-1201 spectrophotometer to determine the optical properties of the films. Moreover, the thickness of the as-grown and annealed films was measured electromechanically in a Dektak 6M profilometer.

For the electrical characterization, Hall effect measurements were carried out at room temperature. In these measurements, the current was supplied by a Keithley 220 programmable current source, and the voltage was measured by a Keithley 619 multimeter. Walker Magnion Model FFD-4D electromagnet was used to produce magnetic field of 0.9 T kept constant in all measurements. Temperature-dependent dark- and photoconductivity measurements in the temperature range of 100–400 K were performed inside the Janis cryostat, equipped with a cooling system. The samples were illuminated perpendicularly by a halogen lamp during the photoconductivity measurements under different illumination intensities varying in between 20 and 115 mW/cm^2.

3 Results and Discussions

XRD analysis showed that the main diffraction peak at 2θ~26.7°, associated to the (112) direction, reveals the preferred orientation of CAIS films [9]. In addition, the peak in this orientation became the more intense diffraction peak with increasing annealing temperature. No remarkable change was observed in the peak positions of the films with annealing (Fig. 1). Good agreement was found between the crystal patterns obtained from deposited thin film X-ray data and those reported in the literature. The structural parameters reported from this diffraction phase are a=0.5937 nm and c=1.1633 nm [9]. Therefore, the tetragonal distortion for these chalcopyrite materials was found approximately as 0.040.

According to Müller et al. [18], a comparison of the degree of preferred orientation in the samples was done in terms of the texture parameter R_I from the ratio of diffraction peak intensities in the XRD pattern. The R_I values were calculated using the relation given in Eq. 1, in which I_{hkl} represents the diffraction peak intensity of (112) direction for the CAIS films and the denominator covers all the diffraction peaks observed in the XRD pattern.

$$R_I = \frac{I_{hkl}}{\sum_{\text{all peaks}} I_{h'k'l'}}, \tag{1}$$

R_I (112) values were found as 0.77, 0.82, and 0.86 for as-grown and annealed at 350 and 400 °C thin films, respectively. The increase in the texture parameter corresponding to the peak value with increasing annealing temperature is the indication of the improvement in the crystallinity in the film structure [18].

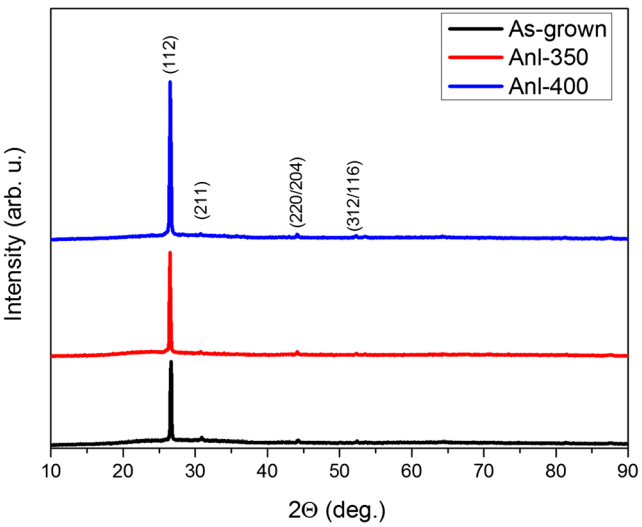

Fig. 1 XRD patterns of CAIS thin films annealed at different temperatures

The compositions of the films were determined by energy dispersive X-ray spectroscopy (EDS), and the results indicated that the deposited films were nearly stoichiometric, within the limit of the experimental error of ±2 %. The EDS data collection was done from several different points on the sample surface, and it was observed that the films were homogenous. The averages of these elemental data for each sample was tabulated in the Table 1, and it can be inferred that post-thermal annealing process caused a small change in the elemental compositions; however, there was only a small amount of decrease in the Se amount in the films. The SEM pictures (see Fig. 2) obtained for the as-grown and annealed films at 350 and 400 °C also confirmed the Se decrease on the surface of the sample, depending on the annealing temperature. As seen in these micrographs, the relatively dark regions on the annealed film surface revealed that there was possible segregation of Se atoms and/or reevaporation from thin film surface due to the high vapor pressure of Se before making the bond to construct the crystalline structure [19]. Moreover, there were Ag agglomerations distributed irregularly and their densities over the surface have decreased with post-annealing. This formation could be due to the diffusion of Ag atoms from the film surface to bulk, or interaction of the nearby segregated Se regions.

The average microcrystalline grain size D was estimated from the XRD pattern using the Scherrer's formula [20] expressed as the following:

$$D = \frac{k\lambda}{\beta\cos\theta}, \tag{2}$$

where k is the shape factor assumed as 0.94 [21], λ is the wavelength of X-rays, β is defined as the diffraction peak width at half height (FWHM), and 2θ is the diffraction angle. This formula express the relation between β and D, and it depends on how the constant of proportionality, k, is determined. Therefore, it can give information about the grain size of the as-grown and annealed CAIS films. It was calculated that the grain sizes of the films increased from 6.3, 8.8, and 12.6 nm, depending on increasing annealing temperature from 350 to 400 °C. It is not so easy to observe such a particular small change in the grain size by using the SEM images.

Table 1 EDS results of as-grown and annealed CAIS thin films

Sample name	Cu (at.%)	Ag (at.%)	In (at.%)	Se (at.%)
As-grown	15.4	16.9	20.3	47.4
Anl-350	16.4	16.7	22.0	44.9
Anl-400	17.8	18.1	22.5	41.6

Moreover, the thicknesses of the films were measured electromechanically by using a profilometer, and they were found to be about 460, 430, and 410 nm, for the as-grown and annealed films at 350 and 400 °C, respectively.

Transmission measurements were carried out in 300–1100 nm regions at room temperature. According to Fig. 3, it can be inferred from the transmittance measurements that there was an enhancement in the transmission when CAIS thin films were subjected to the annealing process. The absorption coefficient (α) of the samples was calculated using the transmission values by means of the relation:

$$\alpha(\lambda) = -\frac{1}{d}\ln\left(\frac{1}{T(\lambda)}\right), \tag{3}$$

where $T(\lambda)$ is the normalized transmittance and d is the thickness of the film. From this expression, the absorption coefficients of the films were found to be in the range of 2.5×10^4–3.5×10^4 cm^{-1}, in the the visible region. The absorption coefficient for a direct band gap transition as a function of the photon energy can be expressed as follows:

$$(\alpha h\nu) = A\left(h\nu - E_g\right)^{1/2}, \tag{4}$$

where A is an energy-independent constant and E_g is the band gap energy. From the plot of $(\alpha h\nu)^2$ versus $h\nu$ (Fig. 4), the band gap values were defined by extrapolation of the straight line on the energy axis. Therefore, the direct band gap energy values of CAIS samples were obtained as about 1.38, 1.41, and 1.45 eV for as-grown and annealed samples at 350 and 400 °C, respectively. In general, decrease in disorder and defect density in the structure results in an increase in the optical band gap [22], and this result is in good correlation with the texture coefficient and grain size analysis.

In the electrical characterization, room temperature Hall effect and temperature-dependent dark- and photoconductivity measurements were performed. The conductivity type of all CAIS thin films was determined as p-type by the hot probe technique. The intrinsic defects are the major effects on determining the conductivity, and the most possible reason for such type of conductivity is the Cu vacancy [23]. The hole concentration and mobility of the samples were obtained through the Hall coefficient R_H and the relation between conductivity and mobility, assuming the validity of Ohm's law [24]. The sign of Hall voltage is also related to type of the charge carrier, and this measurement gave the same result with the hot probe analysis. The room temperature Hall mobilities were 0.57, 4.21, and 143.54 cm^2/V s and hole concentrations were 1.16, 2.76, and 5.16×10^{20} cm^{-3} for as-grown and annealed films, respectively. Moreover, the temperature-dependent dark-conductivity measurements were performed to analyze the change in the conductivity values of the CAIS films in different temperatures. As given in Fig. 5, the variation of the

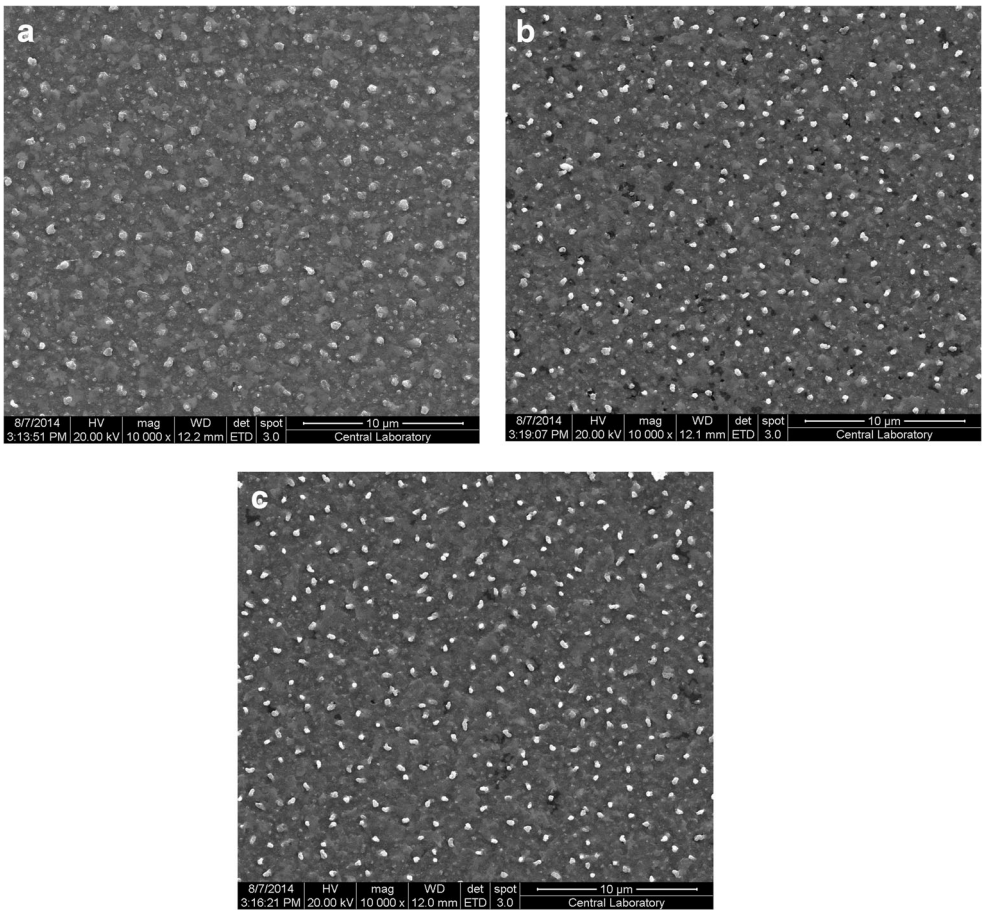

Fig. 2 SEM micrographs for **a** as-grown film, **b** film annealed at 350 °C and **c** at 400 °C

conductivity as a function of temperature showed an increasing behavior with increasing absolute temperature for the as-grown thin film. On the other hand, applying post-thermal process, the semiconductor properties of the CAIS films were transformed into a degenerate form, along with the increase in conductivity because of segregation and/or reevaporation of Se atoms in the structure [25]. Although there was no distinct variation in the composition of the films, changes in the surface morphology of the films with annealing could be the reason for this type of measurements. Room temperature electrical conductivity values were obtained as 1.12, 5.98, and 9.83 Ω cm^{-1} for as-grown and annealed at 350 and 400 °C thin films, respectively. Therefore, it is clear from the conductivity measurements that higher annealing

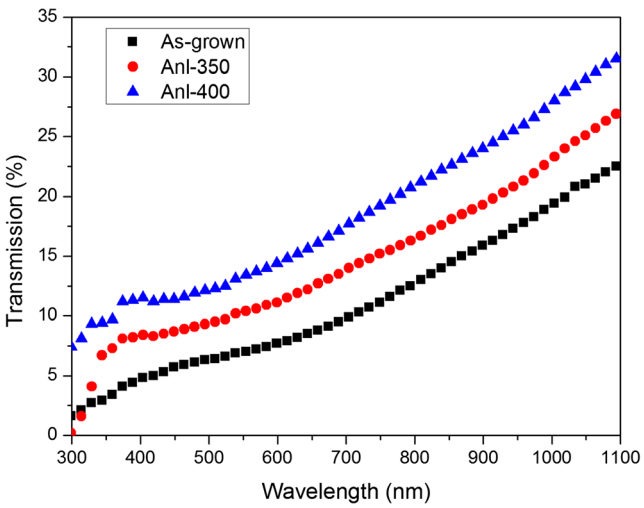

Fig. 3 Transmission spectra for CAIS thin films

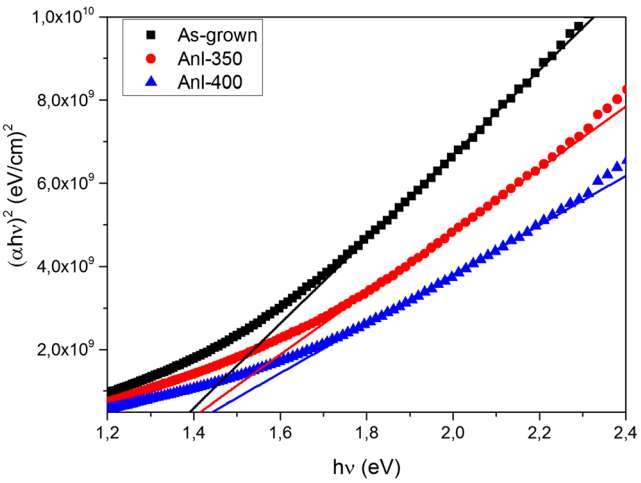

Fig. 4 Variation of absorption coefficient with the photon energy for CAIS thin films

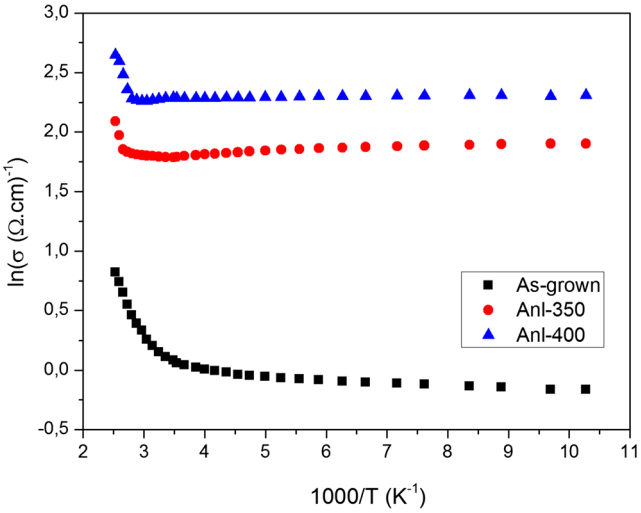

Fig. 5 Temperature-dependent electrical conductivity of as-grown and annealed CAIS thin films at 350 and 400 °C

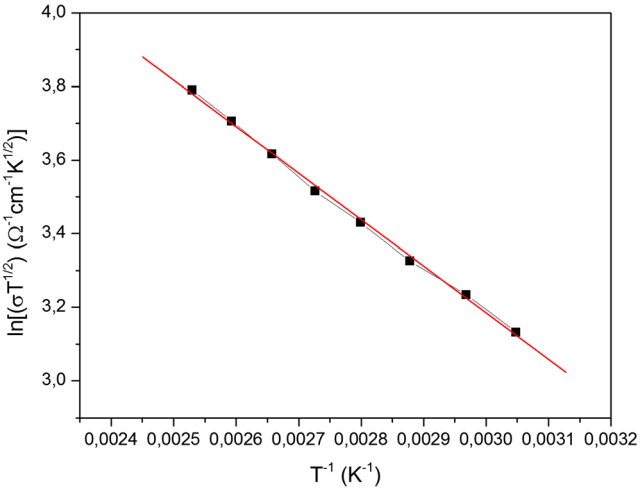

Fig. 6 Plots of $\ln(\sigma T^{1/2})$ versus T^{-1} in the high-temperature region for the as-grown CAIS film. *Solid lines* are the best fit lines according to Eq. 5

temperature results in low-resistive samples, as a result of the structural modifications [25]. This systematic decrease in resistance values for the films could be related with the increase in surface metallic behavior.

Consequently, only for as-grown CAIS film, the variation of conductivity as a function of temperature showed a distinct semiconductor characteristic, and the observed different linear regions in this variation can be taken as the indication of existence of different conduction mechanism dominating in different temperature regions with different activation energies [26]. Since the deposited films were not intentionally doped, the variation in the conductivity mechanism was possibly due to the intrinsic defects [27]. There were three distinct slopes in the different temperature regimes: 100–230, 240–295, and 310–400 K. Therefore, it is possible to determine the dominant conduction mechanisms for these three distinct temperature regions by applying all possible conductivity mechanism models, calculating the slope of the conductivity versus temperature plot in the straight line region, and determining the maximum correlation coefficient (R^2) of the best fit [28, 29]. The analysis of the high temperature region (in 310–400 K) was given in Fig. 6. According to thermionic conduction mechanism, the conductivity can be expressed as [30]:

$$\sigma(T) = \frac{\sigma_0}{T^{1/2}} \exp\left(-{}^{E_a}/_{k_B T}\right), \tag{5}$$

where σ_0 is the pre-exponential factor, E_a is the conductivity activation energy, and k_B is the Boltzmann's constant. Experimentally, Arrhenius plot was made by using Eq. 5, and the dominant conduction mechanism was obtained as thermionic emission (TE), with $R^2 = 0.98$. From this linear region, the corresponding thermal activation energy was found to be 96.1 meV. On the other hand, variable range hopping (VRH) mechanism became dominant in the low temperature region. By this model, charge carriers cannot pass over the grain boundary potential barrier because of not enough thermal activation energy; hopping can take place between the localized states near the Fermi level [30, 31]. In as-grown CAIS film, the temperature dependence of the electrical conductivity in temperature region of 240–295 K obeyed 3D Mott VRH. According to this model, the conductivity depends on temperature as

$$\sigma(T) = \frac{\sigma_0}{T^{1/2}} \exp\left(-\left({}^{T_{0M}}/_{T}\right)^{1/4}\right), \tag{6}$$

where T_{0M} is the characteristic temperature coefficient. For this region (see Fig. 7), the necessary fitting procedure was applied to the experimental data by using Eq. 6 to determine the characteristic parameters for the hopping conductivity.

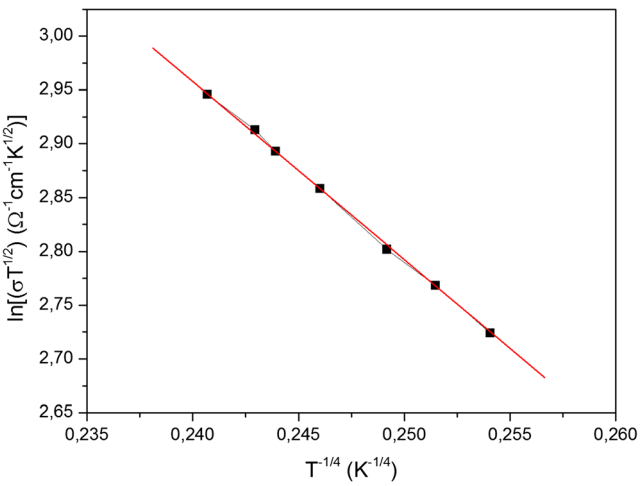

Fig. 7 Plots of $\ln(\sigma T^{1/2})$ versus $T^{-1/4}$ in the low-temperature region for the as-grown CAIS film. *Solid lines* are the best fit lines according to Eq. 6

The parameters related to the Mott VRH were the following: $T_{0M}=7.50\times10^4$ K, α (the coefficient of exponential decay constant of the localized states)$=1.85\times10^7$ cm^{-1}, N_{EF} (the density of localized states at Fermi level)$=1.76\times10^{22}$ eV^{-1} cm^{-3}, R_M (average hopping distance)$=8.30\times10^{-8}$ cm, and W_M (average hopping energy)$=2.38\times10^{-2}$ eV [32]. The fitting and calculated parameters were reasonable within Mott's requirements of the localized state model as $W>k_BT$ and $\alpha R>1$ [15, 33]. However, in the temperature range of 100–230 K, the validity of the Mott's model was not observed due to the limited temperature range of fit. In this region, the electrical conductivity was matched with 3D Efros-Shklovskii (ES) VRH model. As the temperature further decreased, Coulomb effect became important in the conduction mechanism [34]. In ES-VRH model, Coulomb effect serves as a barrier to the conduction process, and the conductivity values can be expressed as follows:

$$\sigma(T)=\frac{\sigma_0}{T^1}\exp\left(-\left({}^{T_{0ES}}/_{T}\right)^{1/2}\right), \tag{7}$$

where T_{0ES} is the characteristic temperature coefficient for ES hopping. As shown in Fig. 8, the fitting process under the ES hopping was in a good agreement with R^2 = 0.99. The parameters related with the Efros-Shklovskii method were $T_{0ES}=8\times10^2$ K, $R_{ES}=2.99\times10^{-8}$ cm, Δ (band width)$=1.74\times10^{-1}$ eV, and $W_{ES}=1.57\times10^{-2}$ eV. The Boltzmann factor results satisfied the VRH requirement as $W>k_BT$, and also the results showed that Δ was comparable to the hopping energy, W_{ES} related with Coulomb potential effect [35].

In addition to the temperature-dependent dark-conductivity, photoconductivity measurements were carried out in the temperature range of 100–400 K. The photoconductivity values were measured under five light intensities ranging from

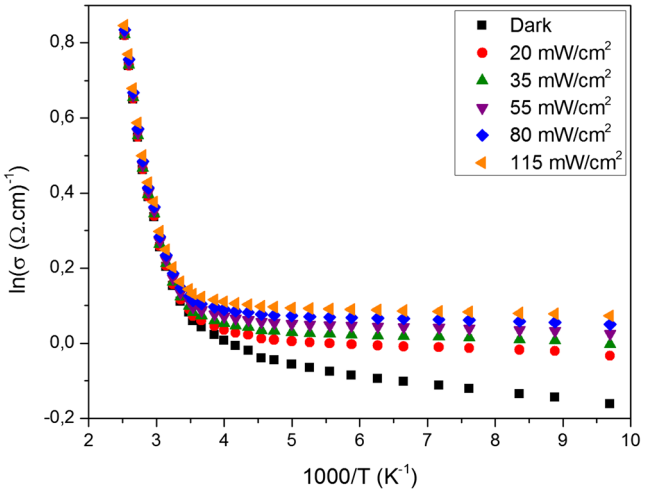

Fig. 9 The variation of the photoconductivity with temperature and illumination intensity for as-grown CAIS thin films

20 to115 mW/cm^2. The photoconductivity variation of the as-grown CAIS thin films with the inverse temperature was plotted in Fig. 9. It shows that the photoconductivity values are greater than the dark-conductivity values. This result indicated that there was an increase in conductivity values with increasing illumination intensity. In order to determine their characteristics, the variation of photocurrent (I_{pc}) as a function of illumination intensity (Φ) was investigated. As shown in Fig. 10, the relation was in the form of $I_{pc}\ \alpha\ \Phi^n$, where the exponent n is a distinctive indicator of the nonequilibrium carriers and characterizes the type of the recombination mechanism [36]. In this case, if it is less than 1, the lifetime decreases with increasing the generation rate, and the behavior of the semiconductor is called sublinear photoconductivity; if it is greater than 1, the lifetime increases with increasing the generation rate. The material becomes more photosensitive with increasing photoexcitation intensities, and this behavior

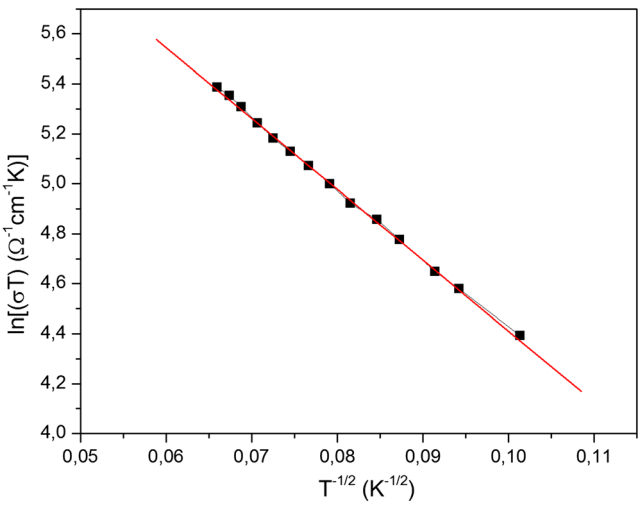

Fig. 8 Plots of ln(σT) versus $T^{-1/2}$ in the low temperature region for the as-grown CAIS film. *Solid lines* are the best fit lines according to Eq. 7

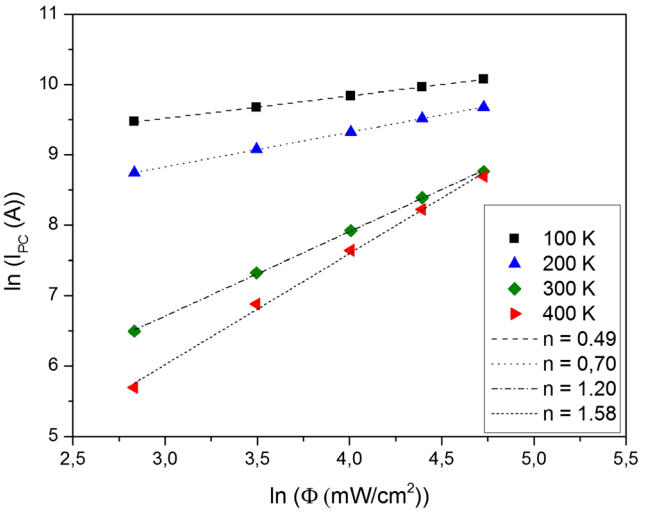

Fig. 10 The variation of the photocurrent as a function of illumination intensity for as-grown CAIS thin films

is called as supralinear photoconductivity [37]. In these measurements, CAIS films changed their behavior from sublinear to supralinear as a function of the temperature. Increasing the exponent *n* values with increasing temperature confirmed the longer lifetimes for free carriers and stronger recombination process at the film surface.

4 Conclusion

In this work the film characteristics of the thermally evaporated CAIS samples were investigated under the effect of post-thermal annealing. According to the XRD analysis, it was determined that the main orientation of the deposited films was along (112) direction and the X-ray diffraction pattern of the films were found in a good agreement with the literature. The main peak became more intended with the annealing process. The compositional analysis showed that the samples at each annealing temperature had nearly stoichiometric composition, within the experimental limits, whereas depending on the increasing annealing temperature, the composition of the samples changed, especially the Se content decreased because of segregation or reevaporation. The room temperature optical measurements were performed on the as-grown and annealed samples, and the band gap energies were obtained as 1.38, 1.41, and 1.45 eV, respectively. The variations in the structural and optical properties of the films were related with structural improvement initiated with the annealing processes. In addition, at room temperature, the Hall effect measurements showed that the mobility and hole concentration increased with annealing. Temperature-dependent dark electrical conductivity measurements showed that, with annealing, the electrical characteristic of the CAIS films were transferred into a degenerate semiconductor behavior. Therefore, only the electrical conduction mechanism of the as-grown CAIS film was analyzed. The experimental results showed a transition from the VRH conduction at low temperatures to the thermionic conduction at higher temperatures. Moreover, the photoconductivity measurements showed that the samples were not high photosensitive. The dependence between the photocurrent and the illumination intensity indicated that CAIS films changed its behavior from sublinear to supralinear as a function of the temperature.

Acknowledgments The authors would like to thank to TUBITAK-BIDEB for the financial supports during this study.

References

1. I.V. Bodnar, V.F. Gremenok, I.A. Viktorov, J. Appl. Spectrosc. **69**, 413–7 (2002)
2. G.V. Rao, G.H. Chandra, P.S. Reddy, O.M. Hussain, K.T.R. Reddy, S. Uthanna, J. Optoelectron. Adv. Mater. **4**, 387–92 (2002)
3. L.L. Kazmerski, Int. Mater. Rev. **34**, 185 (1989)
4. P. Malar, S. Kasiviswanathan, Sol. Energy Mater. Sol. Cells **88**, 281–92 (2005)
5. S. Wagner, J.L. Shay, P. Migliorato, H.M. Kasper, Appl. Phys. Lett. **25**, 434 (1975)
6. T. Minemoto, T. Matsui, H. Takakura, Y. Hamakawa, T. Negami, Y. Hashimoto, T. Uenoyama, M. Kitagawa, Sol. Energy Mater. Sol. Cells **67**, 83 (2001)
7. B.J. Stanbery, Crit. Rev. Sol. Stat. Mater. Sci. **27**, 73 (2002)
8. S.A. Little, V. Ranjan, R.W. Collins, S. Marsillac, Appl. Phys. Lett. **101**, 231910 (2012)
9. G.V. Rao, G.H. Chandra, O.M. Hussain, S. Uthanna, B.S. Naidu, J. Alloys Compd. **325**, 12–7 (2001)
10. G.V. Rao, G.H. Chandra, P.S. Reddy, O.M. Hussain, K.T.R. Reddy, S. Uthanna, Vacuum **67**, 293–8 (2002)
11. I.V. Bodnar, I.A. Viktorov, S.L. Sergeev-Nekrasov, Cryst. Res. Technol. **33**, 885–90 (1998)
12. J.G. Albornoz, R. Serna, M. Leon, J. Appl. Phys. **97**, 103515 (2005)
13. A.A. Lavrentyev, B.V. Gabrelian, I.Y. Nikiforov, R.R. Rehr, A.L. Ankudinov, Phys. Scr. **T115**, 212–4 (2005)
14. A.R. Aquino, A. Rockett, S.A. Little, S. Marsillac, Proceedings of the 35th IEEE Photovoltaic Specialists Conference (PVSC) 003386–003390 (2010)
15. A.R. Aquino, S.A. Little, S. Marsillac, R. Collins, A. Rockett, Proceedings of the 37th IEEE Photovoltaic Specialists Conference (PVSC) 003532–003536 (2011)
16. N.S. McAlpine, P. McConville, D. Haneman, L. Chernyak, D. Cahen, J. Appl. Phys. **79**, 7370–2 (1996)
17. G.V. Rao, G.H. Chandra, O.M. Hussain, S. Uthana, B.S. Naidu, Cryst. Res. Technol. **36**, 571–6 (2000)
18. J. Muller, J. Nowoczin, H. Schmitt, Thin Solid Films **496**, 364 (2006)
19. A. Roth, *Vacuum technology*, 2nd edn. (North Holland, Amsterdam, 1980)
20. E.F. Kaelble, *Handbook of X-rays* (McGraw-Hill, USA, 1967)
21. J.I. Langford, A.J.C. Willson, A. Survey, J. Appl. Crystallogr. **11**, 102 (1978)
22. M. Parlak, C. Erçelebi, Thin Solid Films **322**, 334–9 (1998)
23. J.L. Shay, J.H. Wernick, *Ternary chalcopyrite semiconductors: growth, electronic properties, and application* (Pergamon, Great Britain, 1975)
24. E.H. Putley, *The Hall effect and semi-conductor physics* (Dover, New York, 1960)
25. T. Colakoglu, M. Parlak, J. Phys. D. Appl. Phys. **42**, 035416 (2009)
26. H. Karaagac, M. Parlak, J. Mater. Sci. Mater. Electron. **22**, 1426–32 (2011)
27. H. Karaagac, M. Kaleli, M. Parlak, J. Phys. D. Appl. Phys. **42**, 165413 (2009)
28. T. Mise, T. Nakata, Thin Solid Films **518**, 5604–9 (2010)
29. J.Y. Seto, J. Appl. Phys. **46**, 5247 (1975)
30. N.F. Mott, E.A. Davis, *Electronic processes in non-crystalline materials* (Clarendon, Oxford, 1979)
31. J. Singh, *Electronic and optoelectronic properties of semiconductor structures* (Cambridge University Press, New York, 2003)
32. R. Singh, R.P. Tandon, G.S. Singh, S. Chandra, Evaluation of Mott's parameters in BF^{-} doped polypyrrole films. Philos. Mag. B. **66**, 285–91 (1992)
33. D.K. Paul, S.S. Mitra, Phys. Rev. Lett. **31**, 1000–3 (1979)
34. S. Lamba, D. Kumar, Phys. Rev. B **59**, 4752–65 (1999)
35. B.I. Shklovskii, A.L. Efros, *Electronic properties of doped semiconductors* (Springer, Heidelberg, 1984)
36. R.H. Bube, *Photoelectronic properties of semiconductors* (Cambridge University Press, Cambridge, 1992)
37. R.H. Bube, *Photoconductivity of solids* (Wiley, New York, 1960)